Electromechanical-mnemonic effects in BiFeO3 for electric field history dependent crystallographic phase patterning

Neumayer, S. M., Browne, N., Naden, A. B., Edwards, D., Mazumdar, D., Bassiri-Gharb, N., Kumar, A., & Rodriguez, B. J. (2018). Electromechanical-mnemonic effects in BiFeO3 for electric field history dependent crystallographic phase patterning. *Journal of Materials Science*, *53*(14), 10231–10239. https://doi.org/10.1007/s10853-018-2278-4

Published in:
Journal of Materials Science

Document Version:
Peer reviewed version

Queen's University Belfast - Research Portal:
Link to publication record in Queen's University Belfast Research Portal

To be submitted to Journal of Material Science

Electromechanical-mnemonic effects in $BiFeO_3$ for electric field history dependent crystallographic phase patterning

S.M. Neumayer[1], N. Browne[2], A.B. Naden[2], D. Edwards[2], D. Mazumdar[3], N. Bassiri-Gharb[4], A. Kumar[2] and B.J. Rodriguez[1*]

[1] School of Physics and Conway Institute, University College Dublin, Ireland

[2] Centre for Nanostructured Media, School of Mathematics and Physics, Queen's University of Belfast, UK

[3] Department of Physics, Southern Illinois University, Carbondale, USA

[4] School of Materials Science and Engineering and George W. Woodruff School of Mechanical Engineering, Georgia Institute of Technology, Atlanta, USA

*brian.rodriguez@ucd.ie

Strained bismuth ferrite thin films unite a wealth of functional properties including ferroelectricity, ferromagnetism, electrooptic coupling and interface-mediated conductivity. The coexistence of rhombohedral (R) and tetragonal (T) phases in these films further contributes to their versatility, as structural transitions can modify functional behaviour and be leveraged to engineer properties such as electrochromism, magnetic characteristics, electromechanical response and charge transport. However, potential device applications necessitate precise control of the location and size of R and T phases and associated microstructures. Here, distinct R/T phase patterns of different spatial expanse are obtained by appropriately pre-poling the film by applying an electric field with an atomic force microscope tip during scanning, which also leads to initially uniform T phases as well as through local application of a certain sequence of voltage pulses. Moreover, the impact of field history on ferroelectric characteristics is investigated, providing further opportunities to tailor functional behavior.

Keywords

Bismuth ferrite, multiferroics, phase transition, first order reversal curve spectroscopy, atomic force microscopy

Introduction

Multifunctional bismuth ferrite (BFO), with coupled magnetic, electromechanical, semiconducting and nonlinear optical properties at room temperature, is a promising material for applications ranging from magnetoelectric information storage, spintronic devices, nano- and micro-electromechanical systems, to switchable diodes and integrated electrooptical and electroacoustic elements [1–9].

In its bulk form, BFO adopts a rhombohedral crystal structure [10] and a metastable tetragonal phase has been predicted theoretically [11–13]. When grown epitaxially on substrates with a large lattice mismatch such as $LaAlO_3$, the BFO film is compressively strained along the in-plane directions [14]. For very thin films, this results in an expansion of the *c*-axis to a monoclinic phase that is approximately tetragonal [15]. Beyond ~ 50 nm as in the films discussed herein, a second monoclinic phase is present and is approximately rhombohedral [14]. For brevity, we refer to these as T- and R-phase, respectively. T- and R-phase have been observed experimentally by both X-ray diffraction [14, 16] and scanning transmission electron microscopy [14]. Further increases in film thickness result in a greater proportion of R-phase (with a correspondingly reduced T-phase population) as the epitaxial strain is relaxed. Despite such pronounced structural distortions, these films appear to be free from grains [17], grain boundaries [18] and dislocations [19], which are common in highly strained heteroepitaxial systems. Exposure to electric fields can induce crystallographic phase transitions from mixed RT phases to pure T phase and vice versa [2–4, 20–23]. Crystallographic phase coexistence and transitions govern a variety of material properties, which unlock opportunities to tailor functional responses. For example, the strong electromechanical coupling of mixed phase BFO [22, 24] can enable lead-free micro-sensors and -actuators for biological applications, while its giant elastic tunability can be exploited in frequency-agile electroacoustic devices [2, 21, 25]. Enhanced conductivity at domain walls and phase boundaries [1, 7, 8, 20, 26, 27] are envisioned to play a role in future nanoelectronic systems such as domain wall based memristors. Electrochromism and optical absorption both depend on crystallographic phases, yielding novel opportunities in photonics and acoustooptic

applications [3]. Moreover, magnetic moments depend on the crystallographic phase, enabling electric control of magnetic properties [4]. These envisioned applications are based on tailored functionality originating from phase-dependent characteristics and the interfaces that can be engineered between R and T phases. Progress in this field requires techniques capable of controlling the size and location of R and T phases and associated microstructures, over several length scales [4].

Here, we demonstrate how the mnemonic effect, *i.e.*, a full history of multiple electric field applications, can be leveraged for precise patterning of RT phases and associated microstructures, thus tailoring material functionality at the (sub-) micrometer length scale. The impact of electric field history was studied by (i) pre-poling two film areas during atomic force microscopy (AFM) scanning with applied dc voltages (V_{dc}) of opposite polarity to obtain specific crystallographic phases and polarization orientation and subsequently, application of (ii) first order reversal curve (FORC) [28–30] spectroscopy.

Materials and methods

Pulsed laser deposition was used to grow ~50 nm-thick epitaxial BFO films on 5 nm thick lanthanum strontium cobaltite electrodes on (001)-oriented lanthanum aluminate substrates [14]. AFM experiments were performed using an Asylum Research AFM (Cypher) and conductive Nanosensors tips (PPP-EFM) with a nominal resonance frequency of 75 kHz and nominal force constant of 2.8 N/m. Piezoresponse force microscopy (PFM) was conducted near the contact resonance (~330 kHz) at an excitation voltage of 1 V using a Zurich Instruments lock-in amplifier (HF2LI). Two different 2×6 μm^2 regions were pre-poled by applying ±9 V, while scanning with a scan rate of 0.5 Hz. Moreover, a uniform T phase was obtained in these areas. FORC spectroscopy allows tracking of the hysteretic evolution of the piezoresponse in the material by applying asymmetric triangular field sweeps of progressively increasing amplitudes, anchored at the saturation voltage, V_{dc}. A train of V_{dc} pulses following a waveform envelope starting and ending at approximately ±7 V was applied in a grid of 15×15 points across pre-poled and pristine areas. Each of the 7 cycles of increasing amplitude consisted of 40 V_{dc} steps. Pre-poling and FORC were performed with a setpoint force of ~100 nN. FORC spectroscopy was conducted in band excitation mode [31–33]. Following data acquisition, simple harmonic oscillator fitting

allowed piezoresponse amplitude, phase, resonance frequency and quality factor to be extracted. The amplitude of the excitation voltage was 1 V and the frequency band was centered around the first harmonic contact resonance. A National Instruments module (PXIe-6124) in combination with a chassis (PXIe-1073) and connector block (BNC-2110) controlled via a LabView interface was used to apply V_{dc} waveforms and record the resulting piezoresponse. Data analysis was performed using Matlab. V_{dc} scans were performed on two 6×6 μm^2 regions with a scan rate of 0.5 Hz starting with a voltage of 0 V, which was increased/decreased to +9 V/-9 V in steps of 1 V every 500 nm along the slow scan axis.

Results and discussion

The as-grown strained BFO thin film is of a uniform negative (downwards) polarization. Due to the large difference of ~ 0.6 Å in the *c*-axis lattice constant between the T- and R-phases [14], the surface of the film is corrugated, as can be seen in the topography image in Figure 1(a). Here, the R-phase appears as darker stripes embedded in a T-phase matrix, subsequently referred to as RT patterns. PFM images show the highest piezoresponse amplitude in the R phase, which has previously been ascribed to a combination of changes in the lattice structure and strain gradients, as well as contributions arising from phase boundaries [21]. It has previously been demonstrated that as-grown RT patterns in BFO films can undergo structural phase transitions via electrostriction when subjected to electric fields [14, 23]. In order to study the effect of the electric field history on the mixed phase microstructure and the resulting functional properties, we study the film in three different states, as shown in the PFM images in Figure 1b. The left area was scanned with a supracoercive voltage of +9 V, resulting in $R_{down} \rightarrow T_{down}$ transitions with out-of-plane polarization parallel to the as-grown film. The right area was scanned with -9 V and shows a 180° rotation of the out-of-plane polarization to the positive polarization direction (upwards and antiparallel to the as-grown film) with pure T phase, T_{up} (Figure 1(b)), *i.e.*, $RT_{down} \rightarrow T_{up}$ transitions. Scanning the left area with +9 V results only in a crystallographic transition to pure T phase, T_{down}. The right area is scanned with -9 V and shows a change to positive polarization (upwards), with pure T phase, T_{up} (Figure 1(b)). The terraces observed within T_{down} and T_{up} regions are ~ 4 Å in height, indicating an absence of grain boundaries as T-phase monolayers extend over tens of microns. These observations are consistent with

previous reports [3, 4, 14, 34]. No voltage was applied to the middle area, which therefore remains in its pristine mixed phase with downward polarization, RT_{down}, and serves as a control area. Elongated continuous RT stripe patterns form in the direction of the boundary between T_{up} and pristine RT_{down} areas.

To induce RT phase patterns and study the evolution of electromechanical behaviour as influenced by pre-poling, FORC spectroscopy was subsequently performed on a 15×15 grid over pristine and positively and negatively pre-poled areas. The V_{dc} waveform used and the resulting topography and PFM images are shown in Figure 1(c). It is evident that pre-poling strongly impacts the resulting polarization state as well as the crystallographic phase pattern. After application of the FORC probing wave, local, highly confined R phase regions (diameter of ~150-200 nm) appear – with direct correspondence to the probed grid points. Additionally, small striped R regions, embedded in the T_{down} area, are also created in proximity of the above points, similar to the R-phase rosette patterns discussed in the literature [23]. The appearance of these regions is explained by the presence of fringing fields around the AFM tip due to the highly localized nature of the electric field. At voltages below coercive values, these fringing fields cause rotation of the polarization from the $\langle 001 \rangle_c$ pseudocubic axes of the T-phase to the $\langle 111 \rangle_c$ axes of the R-phase, which causes the reversible T → R structural transitions.

In comparison, the R phase stripes in T_{up} region are wider (widths of ~300-400 nm) and expand well beyond the immediate region beneath the AFM tip. Moreover, at FORC-probed locations, the final polarization is reversed (downwards), resulting in circular domain walls. Such domain walls can enhance the formation of new R phase needle domains embedded in the adjoining T phase matrix giving rise to RT patterns, evidence of which is also observed at the boundary between RT_{down} and T_{up} regions. Lastly, the RT_{down} region exhibits more T phase after application of the FORC pulses with respect to the pristine state (highlighted with indictors in Figure SI1 in supplementary information).

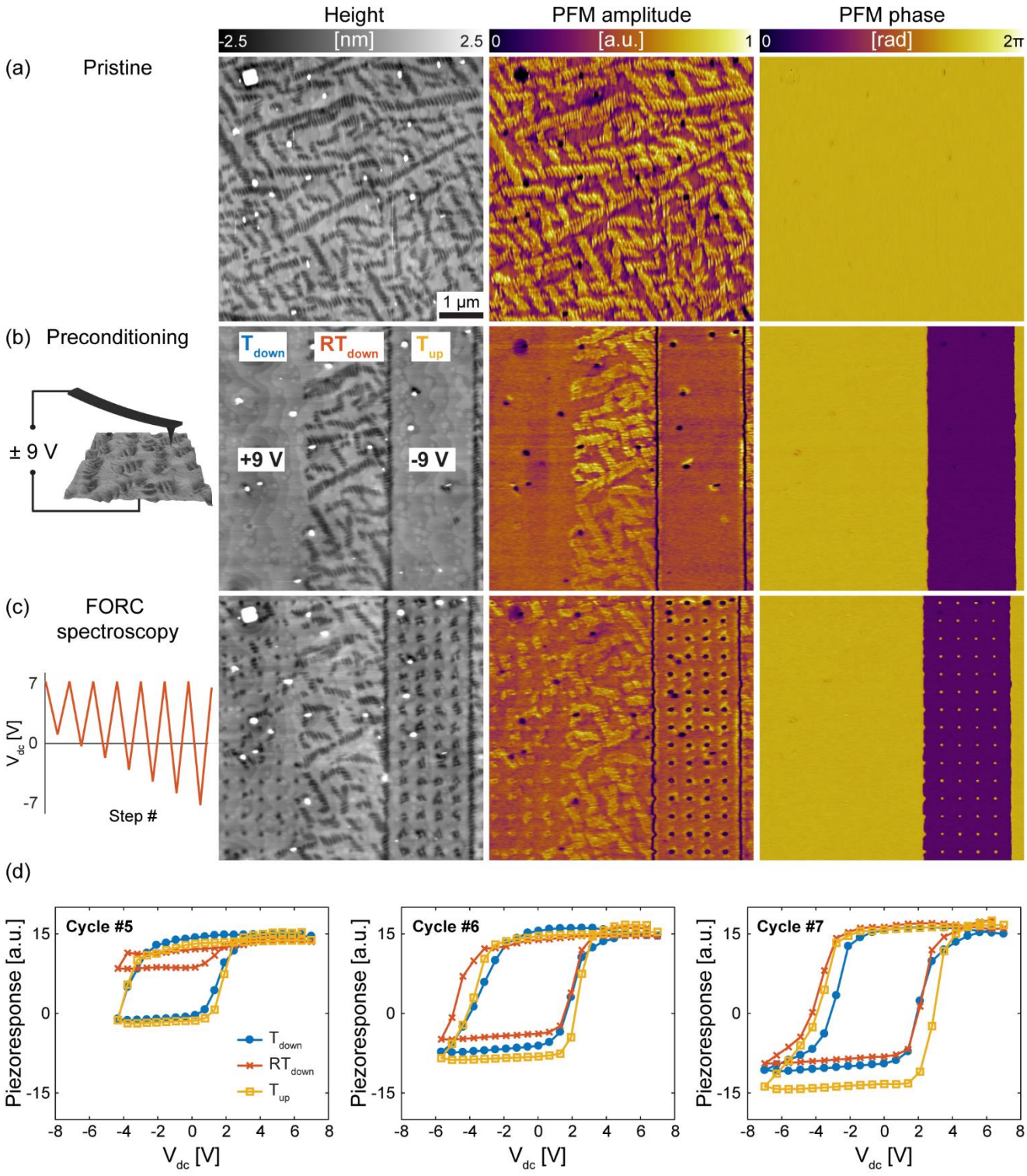

Figure 1 Height and PFM amplitude and phase images of (a) the pristine BFO film, (b) BFO after pre-poling by scanning with +9 V (left area) and -9 V (right area) and (c) BFO after FORC spectroscopy. The envelope of the

applied FORC waveform is depicted in (c). (d) FORC piezoresponse loops of cycle #5, #6 and #7 averaged over pre-poled and pristine areas.

To gain insight into the impact of pre-poling on the evolution of electromechanical behavior, FORC piezoresponse loops were extracted and averaged over the pre-poled areas, T_{down} and T_{up}, as well as the pristine region, RT_{down}. Significant loop opening, indicating the onset of switching, could be observed starting from cycle #5 within a voltage range between +7 V and -4.33 V (Figure 1(d)). While T_{up} and T_{down} exhibit very similar loop shapes, the area of pristine RT_{down} loops are initially much smaller than the others. This is likely caused by the fact that the as-grown film is in its natural equilibrium state and is therefore less susceptible to subcoercive structural phase transitions whereas the pre-conditioned T-phase regions both constitute new metastable states. In other words, the as-grown region represents a minimum energy state for the film and thus requires more energy (*i.e.*, greater electric field) to reorganize than the new, higher energy pre-conditioned regions.

Starting in cycle #6 (between +7 V and -5.67 V) the three loops are very similar in shape and size as all pixels switch within the applied V_{dc}. In cycle #7 (between +7 V and -7 V), piezoresponse loops continue to grow in height and show lowest coercive voltages for T_{down}, whereas T_{up} exhibits the highest value. Therefore, even after multiple polarization switching cycles, pre-poling appears to influence ferroelectric response to the applied voltage waveform between ±7 V. However, bulk measurements over larger length scales might show different behavior than in these single point switching experiments as the polarization of the surrounding material can affect ferroelectric switching as well as phase transitions. As touched upon above, the linked processes of polarization switching and phase transitions occur in a stepwise manner and it is well known that in systems that undergo such transitions, the path of least energy for 180° polarization rotation of the T-phase is via intermediate $\langle 111 \rangle$ rhombohedral directions. Starting with T_{down}, for example, the route is ultimately $T_{down} \rightarrow R_{down} \rightarrow R_{up} \rightarrow T_{up}$. Therefore, the effects of preconditioning are to change the initial state of the points interrogated by FORC and to alter the boundary conditions surrounding these points, *i.e.*, whether the polarization is parallel or antiparallel to the applied electric field.

If FORC spectroscopy is performed using a waveform that starts and ends at +9 V (with a minimum value of -9 V), the resulting RT patterns of the three pre-poled areas are more similar and the R phase in T_{down} is less confined than for lower voltages (SI Figure SI2(a)). At these higher voltages, differences in electromechanical behaviour of the three pre-poled areas are small, especially for cycle #5 (between +9 V and -6 V) and cycle #6 (between +9 V and -7.5 V), whereas in the last cycle between ±9 V, T_{up} exhibits a larger loop area (SI Figure 2(b)). In order to obtain confined RT structures it is, therefore, crucial to apply V_{dc} pulses of lower magnitude than the voltage used for pre-poling.

In addition to the voltage magnitude, the polarity of the waveform also affects the resulting RT patterns and consequent ferroelectric properties of the material. For a FORC waveform starting and ending at -7 V (*i.e.*, a waveform anchored at negative instead of positive voltage), an increase in mixed RT phase is observed in all three areas with T_{up} exhibiting slightly better confinement (Figure 2(a)). Since V_{dc} ends at negative voltages, switched ferroelectric domains are visible in T_{down} and RT_{down}, but not T_{up}. Domain size analysis from higher resolution images (see SI Figure 3) shows larger domain areas of 4300 ± 400 nm^2 within T_{up} for the positive waveform (starting and ending at +7 V) and smaller domains within RT_{down} and T_{down} (2500 ± 300 nm^2 and 2300 ± 600 nm^2, respectively) for waveforms starting and ending at negative voltages. The presence of larger domains is consistent with the lower switching voltage in the T_{up} region compared to the other two. However, while the initial structural phase governs ferroelectric switching for the FORC waveform of positive polarity, loop opening depends on the initial polarization orientation if a negative FORC waveform is applied (Figure 2(b)). The effective average piezoresponse is larger for the regions with polarization well-aligned with the direction of probing voltage (*i.e.*, T_{up}), an effect clearly highlighted in the curves well below the coercive value (Cycle #5). At increasing voltage (between -7 V and +5.67 V), loop areas of the different pre-poled regions become more similar, as nearly all pixels of the three areas switch.

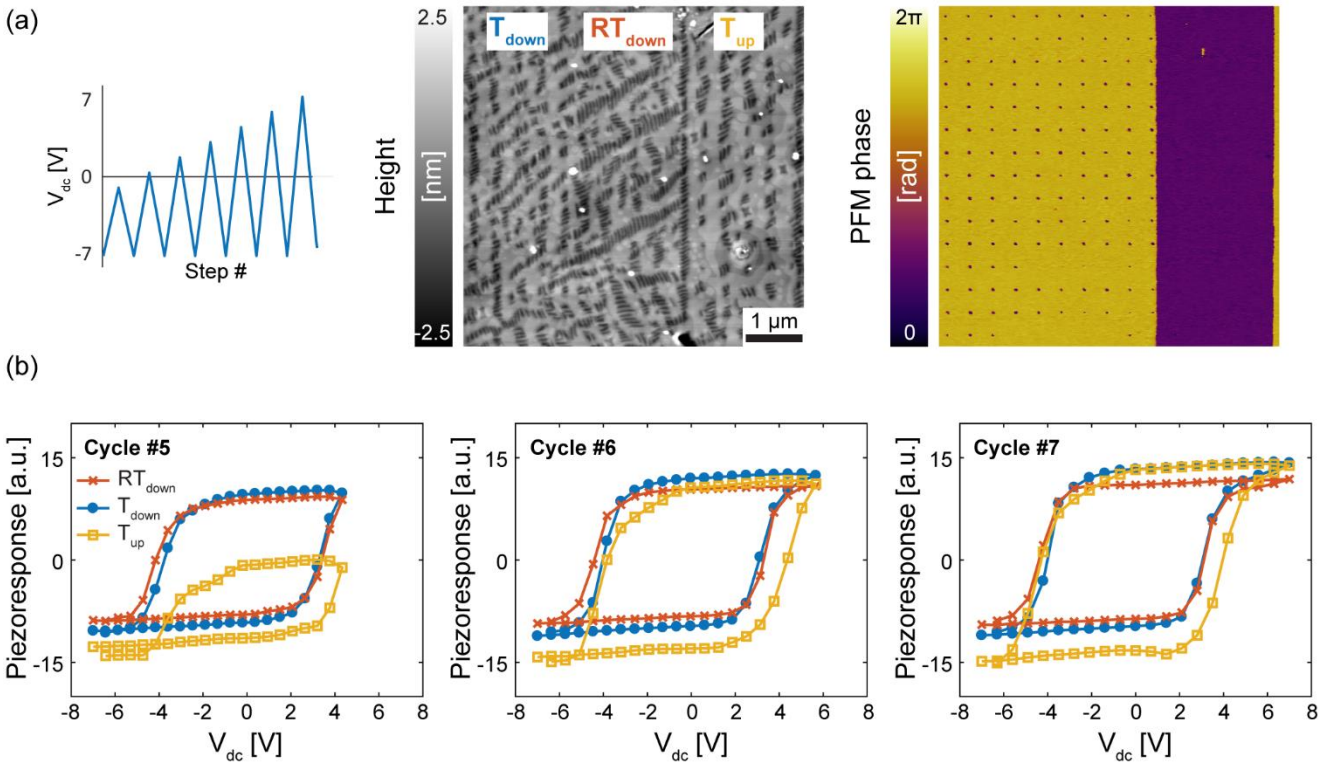

Figure 2 (a) Envelope of the FORC spectroscopy waveform (starting and ending at -7 V) that was applied across pre-poled areas as well as height and PFM phase images showing resulting crystallographic and polarization patterns, respectively. (b) Obtained hysteresis loops for FORC cycles #5, #6 and #7 for the three pre-poled areas.

Since crystallographic patterns and electromechanical behaviour show dependence on FORC waveform polarity and amplitude, the interplay of crystallographic phase change and polarization switching is further probed by scanning the BFO film under application of a dc electric field of increasing magnitude. A negative voltage, decreasing from 0 V to -9 V was applied within one area (Figure 3(a)), whereas a separate area is scanned with positive voltages from 0 V to +9 V (Figure 3(b)). As evident from topography and PFM phase images acquired after V_{dc} scanning, at negative V_{dc}, the appearance of mixed RT phase increases within a range of -3 V to -5 V, beyond which switching from RT_{down} to T_{up} phase occurs. The crystallographic phase transition is therefore accompanied by a change in polarization. It is noted that some persisting islands of R phase remain even at high positive and negative voltages, which might be related to changes in tip – sample contact (*e.g.*, at particles on the surface) or subsurface defects. Although experimental conditions for ferroelectric switching in voltage

spectroscopy and V_{dc} scanning are slightly different (*e.g.,* different field exposure duration, domain growth dynamics), the voltage required for switching observed in FORC loops and bias scans are found to be within a similar range. Sequentially increasing the negative V_{dc} appears to prevent formation of long patterns of RT stripes in the field of view that were previously observed at domain walls (Figure 1). Intriguingly, at positive voltages, transition from RT_{down} to mainly T_{down} occurs from +5 V and higher, but no intermediate regime for enhancement of the RT content is observed. Such observation is in part consistent with the FORC experiments where the positively anchored waveform result in highly confined R phases and previous RT stripes transitioned to pure T phase. According to V_{dc} scanning experiments, the final crystallographic phase after a negative FORC waveform is expected to be T, as -7 V is well beyond the switching and phase transition voltage.

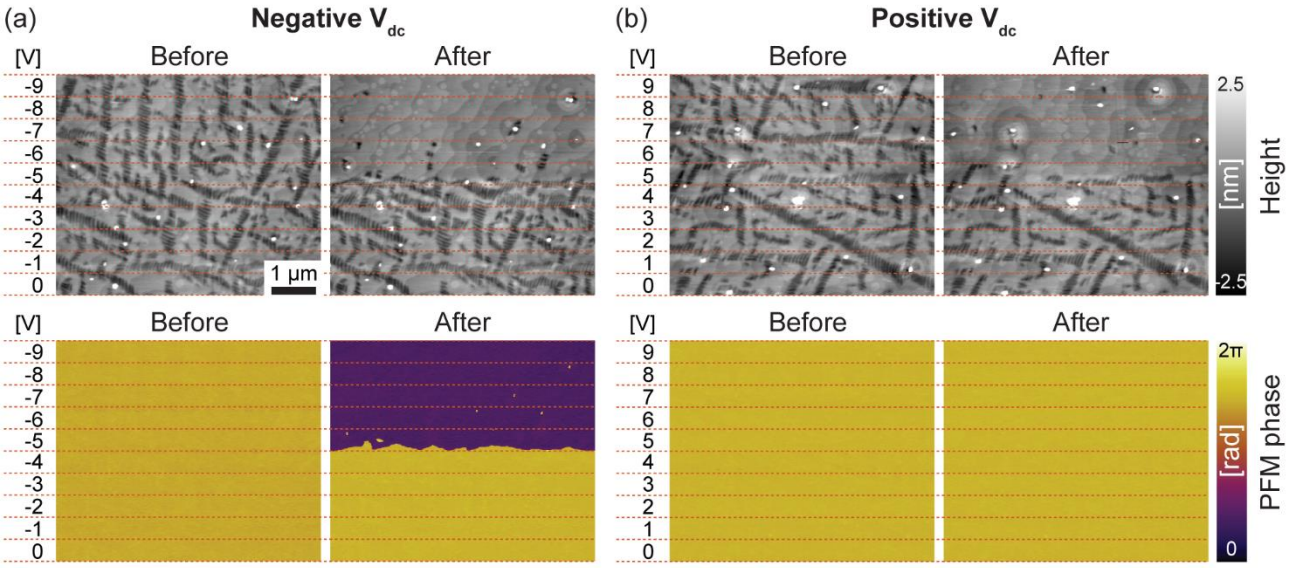

Figure 3 Height and PFM phase images recorded before and after scanning two different sample regions while applying stepwise increasingly positive and negative voltages of (a) 0 V to -9 V and (b) 0 V to +9 V. Dashed lines indicate the voltage applied to a certain image area.

This contradiction suggests that the whole electric field history has an impact on the resulting RT patterns in mixed phase BFO films, rather than only the final voltage step. Moreover, literature suggests that for strained BFO, polarization switching in T phase is mediated by the R phase and, therefore, ferroelectric switching occurs

in the sequence $T_{down} \rightarrow R_{down} \rightarrow R_{up} \rightarrow T_{up}$ from free energy density calculations [20]. However, an R_{up} phase is not observed in V_{dc} scanning experiments of Figure 3, in fact, the mixed RT phase appears always in a negative polarization orientation, whereas the polarization of T depends on poling voltage. Given that the resulting domain patterns in Figure 1(c) contain upwards oriented, mixed RT domains, experimental parameters, specifically the step size of the applied V_{dc}, appear to play a strong role. Therefore, a continuous waveform was used to directly study the structural phase change spectroscopically in a grid across T_{down}, RT_{down} and T_{up} areas.

The V_{dc} waveform as depicted in Figure 4 starts and ends at 0 V. The vertical displacement was simultaneously measured by the AFM z-sensor and indicates structural phase transitions by steep slopes, whereas less drastic changes can be attributed to field and polarization dependent piezoelectric response [20]. Knowing the initial polarization and approximate switching voltages, switching events and polarization states can be inferred from the response of the z-sensor at appropriate applied voltage values. The shown data are extracted from three single points that are representative for their respective areas and are initially in a T phase state. Within these experiments:

(i) Polarization switching is accompanied by structural phase transitions. Simultaneous changes in polarization and structure, as inferred from z displacement, are particularly obvious in the first part of the graph for T_{up} at positive V_{dc}, where switching is only possible in the previously positively poled region. In T_{down} and RT_{down} areas, switching from downwards to upwards polarization in the first cycle appears to cause a structural phase change from T to RT.

(ii) Phase transitions appear similar in T_{down} and RT_{down} but different from T_{up}, highlighting that the initial polarization state governs the resulting RT patterns. Similar observations were made for FORC piezoresponse hysteresis loops (for the waveform starting and ending at -7 V). Furthermore, upon application of continuous V_{dc} waveforms, the RT mixed phase in upwards polarization is apparent in z-sensor data.

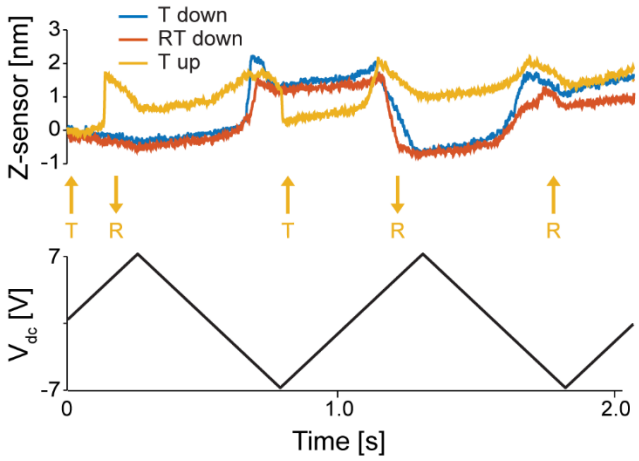

Figure 4 Z-sensor data and applied voltage in spectroscopic measurements extracted from representative pixels in pre-poled and pristine areas. Arrows and labels indicate polarization and phase of T_{up} graph.

The resulting crystallographic and domain patterns (SI Figure SI4) are similar to those observed using the FORC waveform that starts and ends at -7 V, corroborating comparability between experiments. To summarize, strained multiphase BFO was pre-poled by applying the +9 V, 0 V and -9 V during scanning to obtain three areas of different crystallographic phase and polarization orientation T_{down}, RT_{down} and T_{up}. Subsequently, FORC spectroscopy was performed across all three areas. The FORC waveform starting and ending at +7 V resulted in patterns of R phase embedded in T with high confinement within the T_{down} area whereas the spatial expanse of alternating RT stripes is higher for $T_{up.}$. Low confinement of RT patterns is also observed for the sequence of FORC pulses that starts and ends at -7 V and the continuous waveform ending with a V_{dc} ramp from -7 V to 0 V. Spectroscopic measurements using the continuous waveform as well as V_{dc} scanning showed that polarization switching is accompanied with a change in crystallographic phase. Moreover, the electromechanical behavior depends on pre-poling as well as polarity and amplitude of FORC waveform.

Conclusions

In conclusion, the spatial extension of mixed RT phase patterns embedded in a uniform T phase can be controlled across several hundred nm via the electromechanical-mnemonic effect through pre-poling of the

sample by scanning with a biased tip and applying a certain sequence of voltage pulses. Moreover, the amplitude and polarity of an asymmetric FORC waveform governs RT stripe formation. Varying the grid density across areas might provide a path to tailor magnetic and optical properties of larger regions of strained BFO. Moreover, the induced RT phase boundaries yield control over local charge transport [27]. Pre-poling also affects ferroelectric properties such as loop opening and coercive voltages even after multiple switching cycles and allows therefore to modify electromechanical behavior.

Acknowledgements

The authors would like to thank S. Jesse for providing the band excitation acquisition code used in this work. This publication has emanated from research conducted with the financial support of Science Foundation Ireland under the US-Ireland R&D Partnership Programme Grant Number SFI/14/US/I3113. A.N. and A.K. acknowledge support by the Department of Education and Learning, Northern Ireland through the US-Ireland R&D partnership grant no. USI-082. NBG gratefully acknowledges support from US National Science Foundation through grant CMMI-1537262.

References

1. Wang C, Jin KJ, Xu ZT, et al (2011) Switchable diode effect and ferroelectric resistive switching in epitaxial $BiFeO_3$ thin films. Appl Phys Lett 98:1–3
2. Li Q, Cao Y, Yu P, et al (2015) Giant elastic tunability in strained $BiFeO_3$ near an electrically induced phase transition. Nat Commun 6:1–9
3. Sando D, Yang Y, Bousquet E, et al (2016) Large elasto-optic effect and reversible electrochromism in multiferroic $BiFeO_3$. Nat Commun 7:10718
4. He Q, Chu Y-H, Heron JT, et al (2011) Electrically controllable spontaneous magnetism in nanoscale mixed phase multiferroics. Nat Commun 2:225
5. Seidel J, Vasudevan RK, Valanoor N (2016) Topological structures in multiferroics - domain walls, skyrmions and vortices. Adv Electron Mater 2:1500292

6. Alsubaie A, Sharma P, Liu G, et al (2017) Mechanical stress-induced switching kinetics of ferroelectric thin films at the nanoscale. Nanotechnology 28:75709

7. Jeon JH, Joo H-Y, Kim Y-M, et al (2016) Selector-free resistive switching memory cell based on $BiFeO_3$ nano-island showing high resistance ratio and nonlinearity factor. Sci Rep 6:23299

8. Boyn S, Girod S, Garcia V, et al (2014) High-performance ferroelectric memory based on fully patterned tunnel junctions. Appl Phys Lett 104:52909

9. Morelli A, Johann F, Burns SR, et al (2016) Deterministic switching in bismuth ferrite nanoislands. Nano Lett 16:5228–5234

10. Moreau JM, Michel C, Gerson R, James WJ (1971) Ferroelectric $BiFeO_3$ X-ray and neutron diffraction study. J Phys Chem Solids 32:1315–1320

11. Ricinschi D, Yun K, Okuyama M (2006) A mechanism for the 150 μC cm^{-2} polarization of $BiFeO_3$ films based on first-principles calculations and new structural data $BiFeO_3$ films based on first-principles calculations and. J Phys Condens Matter 18:L97

12. Ravindran P, Vidya R, Kjekshus A, et al (2006) Theoretical investigation of magnetoelectric behavior in $BiFeO_3$. Phys Rev B 74:224412

13. Ederer C, Spaldin NA (2005) Effect of epitaxial strain on the spontaneous polarization of thin film ferroelectrics. Phys Rev Lett 95:257601

14. Zeches RJ, Rossell MD, Zhang JX, et al (2009) A strain-driven morphotropic phase boundary in $BiFeO_3$. Science 326:977–980

15. Salluzzo M, Cezar JC, Brookes NB, et al (2009) Orbital reconstruction and the two-dimensional electron gas at the $LaAlO_3/SrTiO_3$ interface. Phys Rev Lett 102:166804

16. Mazumdar D, Shelke V, Iliev M, et al (2010) Nanoscale switching characteristics of nearly tetragonal $BiFeO_3$ thin films. Nano Lett 10:2555–2561

17. Straumal BB, Protasova SG, Mazilkin AA, et al (2016) Ferromagnetic behaviour of ZnO: the role of grain boundaries. Beilstein J Nanotechnol 7:1936–1947

18. Straumal BB, Mazilkin AA, Protasova SG, et al (2015) Grain boundaries as a source of ferromagnetism

and increased solubility of Ni in nanograined ZnO. Rev Adv Mater Sci 41:61

19. Chen Y, Washburn J (1996) Structural transition in large-lattice-mismatch heteroepitaxy. Phys Rev Lett 77:4046–4049

20. Sharma P, Heo Y, Jang B, et al (2016) Structural and electronic transformation pathways in morphotropic $BiFeO_3$. Sci Rep 6:32347

21. Sharma P, Kang KR, Jang BK, et al (2016) Unraveling elastic anomalies during morphotropic phase transitions. Adv Electron Mater 2:1600283

22. Vasudevan RK, Okatan MB, Liu YY, et al (2013) Unraveling the origins of electromechanical response in mixed-phase bismuth ferrite. Phys Rev B - Condens Matter Mater Phys 88:1–7

23. Vasudevan RK, Liu Y, Li J, et al (2011) Nanoscale control of phase variants in strain-engineered $BiFeO_3$. Nano Lett 11:3346–3354

24. Zhang JX, Xiang B, He Q, et al (2011) Large field-induced strains in a lead-free piezoelectric material. Nat Nanotechnol 6:98–102

25. Cao Y, Yang S, Jesse S, et al (2016) Exploring polarization rotation instabilities in super-tetragonal $BiFeO_3$ epitaxial thin films and their technological implications. Adv Electron Mater 2:1600307

26. Seidel J, Maksymovych P, Batra Y, et al (2010) Domain wall conductivity in La-Doped $BiFeO_3$. Phys Rev Lett 105:197603

27. Heo Y, Hong Lee J, Xie L, et al (2016) Enhanced conductivity at orthorhombic–rhombohedral phase boundaries in $BiFeO_3$ thin films. NPG Asia Mater 8:e297

28. Kim Y, Kumar A, Ovchinnikov O, et al (2012) First-order reversal curve probing of spatially resolved polarization switching dynamics in ferroelectric nanocapacitors. ACS Nano 6:491–500

29. Guo S, Ovchinnikov OS, Curtis ME, et al (2010) Spatially resolved probing of Preisach density in polycrystalline ferroelectric thin films. J Appl Phys 108:84103

30. Ovchinnikov O, Jesse S, Guo S, et al (2010) Local measurements of Preisach density in polycrystalline ferroelectric capacitors using piezoresponse force spectroscopy. Appl Phys Lett 96:112906

31. Jesse S, Vasudevan RK, Collins L, et al (2014) Band excitation in scanning probe microscopy: recognition

and functional imaging. Annu Rev Phys Chem 65:519–36

32. Jesse S, Kalinin SV, Proksch R, et al (2007) The band excitation method in scanning probe microscopy for rapid mapping of energy dissipation on the nanoscale. Nanotechnology 18:435503

33. Balke N, Bdikin I, Kalinin S V., Kholkin AL (2009) Electromechanical imaging and spectroscopy of ferroelectric and piezoelectric materials: State of the art and prospects for the future. J Am Ceram Soc 92:1629–1647

34. Damodaran AR, Liang C-W, He Q, et al (2011) Nanoscale sructure and mechanism for enhanced electromechanical response of highly strained $BiFeO_3$ thin films. Adv Mater 23:3170–3175